Large Eddy Simulation of soot evolution in turbulent nonpremixed bluff body flames

Hernando Maldonado Colmán^{a,*}, Pavan Prakash Duvvuri^a, Michael E. Mueller^a

^a Department of Mechanical and Aerospace Engineering, Princeton University, Princeton, NJ 08544, USA

Abstract

Large Eddy Simulation (LES) is utilized to investigate soot evolution in a series of turbulent nonpremixed bluff body flames featuring different bluff body diameters. The modeling framework relies on recent development in the soot subfilter Probability Density Function (PDF) model that can correctly account for the distribution of soot with respect to mixture fraction, correcting errors in previous soot subfilter PDF models that significantly overpredict soot oxidation. With the previous soot subfilter PDF model, no soot was observed outside of the recirculation zone in past studies on similar bluff body flames. Results obtained with the current LES modeling approach compare favorably with the experimental measurements of the flow field and the soot volume fraction. Notably, the current LES modeling approach correctly predicts large soot volume fractions in the recirculation zone, a decrease in the soot volume fraction through the high-strain neck region, and then an increase again in the downstream jet-like region. Consistent with the experimental measurements, the larger bluff body diameter, with its larger recirculation zone with longer residence times, generates more soot in the recirculation zone and also more soot in the highstrain neck region. Analysis of the soot volume fraction source terms lead to mechanistic understanding of soot evolution in the entirety of the bluff body flames. Most of the soot generated in the recirculation zone is oxidized but some escapes unoxidized and is passively transported through the neck region. Virtually no new soot forms in the downstream jet-like region, and the increase in the soot volume fraction in the jet-like region is due to acetylene-based surface growth of the soot transported through the neck region. This mechanism could not be predicted with the previous soot subfilter PDF model, with the recent soot subfilter PDF model being critical in the understanding of this basic mechanism.

Keywords: Soot; Large Eddy Simulation (LES); Bluff body flames; Turbulent nonpremixed flames; Presumed subfilter PDF

1. Introduction

Many practical combustion systems feature fuelrich regions of recirculating flow, whose long residence times promote the undesired formation of soot particulates. To better understand such flows, laboratory-scale configurations with similar flow features have been developed and investigated both experimentally and computationally. Such configurations include swirl flames in confined combustion chambers or bluff body flames. While the former configuration has been studied computationally by numerous groups recently (e.g., [1, 2]), bluff body flames have received far less attention [3, 4].

Mueller et al. [3] conducted for the first time a joint experimental-computational study of a turbulent nonpremixed bluff body flame. In that work, while the experimental measurement campaign considered both the upstream recirculation zone and the downstream jet-like region, the computational component, utilizing Large Eddy Simulation (LES), only considered the upstream recirculation zone. The computational results correctly predicted the low soot intermittency in the recirculation zone and compared favorably for the soot volume fraction with the experimental measurements. Deng et al. [4] conducted a similar joint experimental-computational study in the same configuration and investigated the influence of hydrogen addition to the fuel. Here again, the LES focused exclusively on the recirculation zone and was in good agreement with the corresponding experimental measurements, showing a substantial soot reduction in the recirculation zone compared to the previous case from Mueller et al. [3]. Further analyses lead to the conclusion that the reduction of soot in the recirculation zone was only in part due to the chemical effect of hydrogen addition but more substantially due to the change in the mixture fraction within the recirculation zone, which was considerably leaner with the addition of hydrogen and corresponding increase in the jet velocity to maintain the same Reynolds number.

However, these two previous works did not computationally investigate soot evolution further downstream in the jet-like region, and the reason is simple: their computational model [5] was not capable of correctly capturing soot evolution in turbulent nonpremixed jet flames. Indeed, a later work from Yang et al. [6] showed that the soot subfilter Probability Density Function (PDF) model from Mueller and Pitsch [5] overpredicts soot oxidation in turbulent nonpremixed jet flames and further modeling was needed. Therefore, Yang et al. [6] proposed a soot subfilter PDF model that accounts for the fact that soot oxidation is very fast (in fact, infinitely fast) and observed a substantial increase in the soot volume fraction in turbulent nonpremixed jet flames. More recently, Maldonado Colmán et al. [7] improved this soot subfilter PDF model to consider instead finiterate oxidation of soot, which is able to capture soot leakage across the flame when local turbulent transport rates are fast relative to the soot oxidation rate (e.g., in smoking flames).

In parallel with these model developments, new experimental studies have been carried out by Rowhani and coworkers [8, 9] on three new turbulent non-premixed bluff body flames fueled by an ethylene/nitrogen mixture. The three flames have burners featuring three different bluff body diameters but are otherwise identical. In their first work, they focused on the influence of the bluff body diameter on the flow field characteristics and the overall characteristics of the flame and recirculation zone. In the second work, they concentrated on the interactions between soot and the flow field and evaluated the impact of the bluff body diameters on these features.

The availability of these new experimental data and the flame series has provided the motivation to revisit the bluff body configuration from a computational perspective. Additionally, the new soot subfilter PDF model for finite-rate oxidation will be employed to model the turbulence-chemistry-soot interactions in order to capture soot phenomena in the jet-like region of the bluff body flames. The objective of this work then is to further challenge the combustion and soot models in LES of these turbulent nonpremixed bluff body flames and provide further insights into the mechanisms of soot evolution in both the recirculation zone and jet-like region, including the effect of the bluff body diameter.

The organization of the manuscript is as follows. First, the LES modeling framework is briefly introduced. The experimental configuration is then presented along with the simulation details. The computational results that follow focus on validation against experimental measurements of velocity and soot volume fraction in the flame series and a mechanistic understanding of soot evolution in these bluff body flames.

2. Modeling framework

This section introduces the LES modeling framework for soot evolution in turbulent nonpremixed flames.

2.1. Soot model

An ensemble of soot particles is statistically represented by a Number Density Function (NDF). In this work, a bivariate NDF is chosen to describe the soot particles through their volume and surface area [10]. The Method of Moments is used to solve (the moments of) the Population Balance Equation (PBE), and closure of the moment transport equations is achieved with the Hybrid Method of Moments (HMOM) [10, 11]. The soot model considers source terms from nucleation from Polycyclic Aromatic Hydrocarbons (PAH), condensation of PAH, particle coagulation, acetylene-based surface growth, and oxidation (and oxidation-induced fragmentation) and has been validated in a variety of laminar flames [10–12].

2.2. Combustion model

Combustion is modeled using the Radiation Flamelet/Progress Variable (RFPV) approach for sooting flames [6, 13], which parameterizes the thermochemical state, obtained from the solution of the steady nonpremixed flamelet equations, in terms of the mixture fraction Z, a progress variable C, and a heat loss parameter H. The mixture fraction has a source term \dot{m}_Z to compensate for the local leaning of the mixture due to the removal of PAH species from the gas-phase to form soot, and the source term for the progress variable is modified to account for the local change in the effective fuel due to the removal of PAH species from the gas-phase to form soot [13]. The source term for the heat loss parameter accounts for the removal of PAH from the gasphase (such that H = 0 corresponds to the adiabatic state) as well as radiative heat losses; the latter is modeled using an optically thin gray approach for both gas [14] and soot [15] radiation. The Strain-Sensitive Transport Approach (SSTA) is considered to take into account different effective Lewis for species depending on their characteristic length scales [16]. An additional lumped PAH transport equation is solved to account for their slow chemistry compared to other combustion products in the thermochemical database; the lumped PAH source term is subdivided into chemical production, chemical consumption, and soot formation contributions for closure following the work of Mueller and Pitsch [13].

2.3. Soot-turbulence-chemistry interactions model

The LES governing equations are closed following Mueller and Pitsch [13] by the convolution of the source terms \dot{Q} (or other quantities) against a joint subfilter PDF $\widetilde{P}(\xi_k, M_j)$ of thermochemical scalars ξ_k ($\in \{Z, C, H\}$) and soot scalars M_j :

$$\overline{\dot{Q}}(\xi_k, M_j) = \overline{\rho} \iint \frac{1}{\rho} \dot{Q}(\xi_k, M_j) \widetilde{P}(\xi_k, M_j) d\xi_k dM_j.$$
(1)

Using Bayes' theorem, the joint subfilter PDF is split into two terms: $\widetilde{P}(\xi_k,M_j)=\widetilde{P}(\xi_k)\widetilde{P}(M_j|\xi_k)$. The first term $\widetilde{P}(\xi_k)$ is the subfilter PDF for the thermochemical variables, which is modeled as a beta distribution for the mixture fraction [17, 18]. The second term $\widetilde{P}(M_j|\xi_k)$ is the conditional subfilter PDF for soot described below.

Maldonado Colmán *et al.* [7] recently developed a new soot subfilter PDF model for finite-rate oxidation and validated the model both *a priori* using DNS data and *a posteriori* in an LES of a turbulent non-premixed piloted jet flame. The soot subfilter PDF model is based on the bimodal PDF of Mueller and Pitsch [5], in which the subfilter PDF is decomposed into non-sooting and sooting modes represented by

delta functions:

$$\widetilde{P}(M_j|\xi_k) = \omega \delta(M_j) + (1-\omega)\delta(M_j - M_j^{\star}(Z, \chi_{\rm st})),$$

where ω is the subfilter intermittency. $M_j^\star(Z,\chi_{\rm st})$ is chosen such that \overline{M}_j is obtained upon convolution against the joint subfilter PDF. To account for the distribution of soot with respect to mixture fraction in the presence of finite-rate soot oxidation, the sooting mode is modeled as $M_j^\star(Z,\chi_{\rm st}) = M_j^{\star\star}\mathcal{G}(Z,\chi_{\rm st})$, where

$$\mathcal{G} = \frac{1}{2} + \frac{1}{2} \tanh \left(\frac{Z - (Z_{\text{soot}} + \delta_Z/2)}{\delta_Z/2} \right) . \quad (3)$$

This profile represents a gradual transition from no soot in lean mixtures to soot in rich mixtures, demarcated by $Z_{\rm soot}$, which is the location in mixture fraction space where the rates of soot oxidation and surface growth are equal and varies with the local mixture fraction dissipation rate χ . The width of this transition $\delta_Z = v_Z |\nabla Z|/k_{\rm ox}$, where v_Z is the mixture fraction iso-surface displacement speed [19] and k_{ox} is the soot oxidation rate coefficient, is narrower when soot oxidation is very fast compared to turbulent transport of soot and wider when soot oxidation is slower compared to turbulent transport of soot. When oxidation is infinitely fast, this model recovers the model of Yang et al. [6] with a sharp transition at Z_{soot} . Compared to the previous model of Yang et al. [6], the new model of Maldonado Colmán et al. [7] can accommodate soot leakage into leaner mixtures (i.e., smoking flames).

The subfilter intermittency is obtained with a similar expression to Yang *et al.* [6]:

$$\omega = 1 - \frac{1}{\int \mathcal{G}(Z, \chi_{\rm st}) \widetilde{P}(Z) dZ} \cdot \frac{\overline{M}_{0,0}^2}{\overline{M}_{0,0}^2}, \quad (4)$$

where the integral in the denominator is precomputed and stored in the RFPV database. Note that the subfilter intermittency requires the solution of an additional transport equation for the filtered square of the soot number density [5].

3. Configuration and computational details

In this section, a brief overview of the experimental configuration and computational setup is presented.

3.1. Experimental configuration

Three bluff body burners are considered, which differ only in the bluff body diameter ($D_{\rm BB}$): 38 mm, 50 mm, and 68 mm. The three cases investigated are referred to as ENB-1, ENB-2 and ENB-3, respectively, as in Refs. [8, 9]. The central fuel jet has a diameter of 4.6 mm. In all three cases, the flow parameters are the same. The central fuel jet consists of an ethylene/nitrogen mixture (4:1 in volume) with

a bulk jet velocity of $32.1~\mathrm{m/s}$ and a corresponding Reynolds number $\mathrm{Re}=15,000$. An air coflow has a bulk velocity of $20~\mathrm{m/s}$. Experimental measurements of both velocity using PIV [8] and soot volume fraction using LII [9] are available for comparison with the computational results.

For further details about the geometry of the burners, flow conditions, or experimental measurements, refer to Refs. [8, 9].

3.2. Computational setup

The LES calculations are performed using the NGA code [20, 21], a structured finite difference solver for low Mach number turbulent reacting flows. The grid-filtered LES calculations are conducted in cylindrical coordinates with the same domain for all three flames. The dimensions of the domain are $0.96~\mathrm{m}$ in the streamwise direction and $0.24~\mathrm{m}$ in the radial direction, and the domain is discretized with $384 \times 192 \times 64$ points in the streamwise, radial, and circumferential directions, respectively. The grid is stretched in both the streamwise and the radial directions. The inlet boundary condition for the central jet is generated from a separate simulation of non-reacting periodic pipe flow with the same bulk velocity. A uniform velocity profile without any turbulent fluctuations is considered for the coflow. This approach follows the basic strategy of previous work [3], and further analysis of the sensitivity to the inflows characteristics are warranted but beyond scope of this work.

The subfilter stress and scalar flux terms are closed using Lagrangian dynamic Smagorinsky(-like) models [22, 23].

The RFPV thermochemical database consists of solutions to the nonpremixed steady flamelet equations and precomputed using FlameMaster [24]. The gas-phase kinetics consists of 1804 reactions and 158 species, including PAH species up to four aromatic rings ($C_{18}H_{10}$), which are all utilized for soot inception [25, 26].

4. Results

The results are divided into three parts. In the first two parts, the results are validated against the experimental measurements of the flow field [8] and of the soot volume fraction [9]. In the final part, the source terms are analyzed to understand how soot evolves in the different regions of the bluff body flame and how this varies with the bluff body diameter.

4.1. Flow field

Figure 1 shows the comparison between the computational results and the experimental measurements [8] of the mean axial and radial velocities; the corresponding root-mean-square velocities are compared in Fig. 2. The first two stations are within the

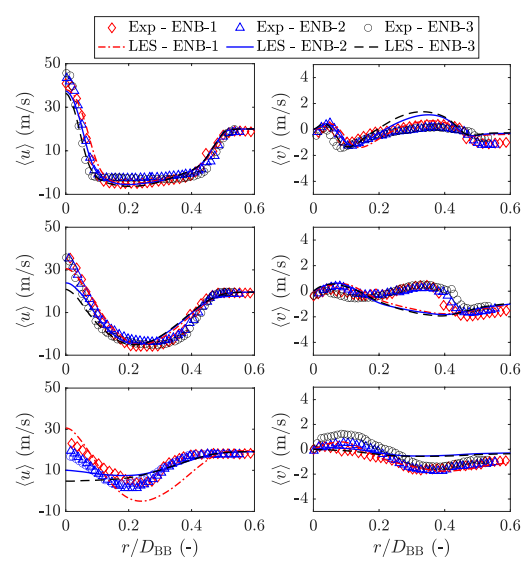


Fig. 1: Radial profiles of the mean axial (left) and radial (right) velocities at three streamwise locations: $x/D_{\rm BB}=0.3$ (top), $x/D_{\rm BB}=0.9$ (middle), and $x/D_{\rm BB}=1.8$ (bottom). The LES results are indicated with lines and the experimental measurements with symbols.

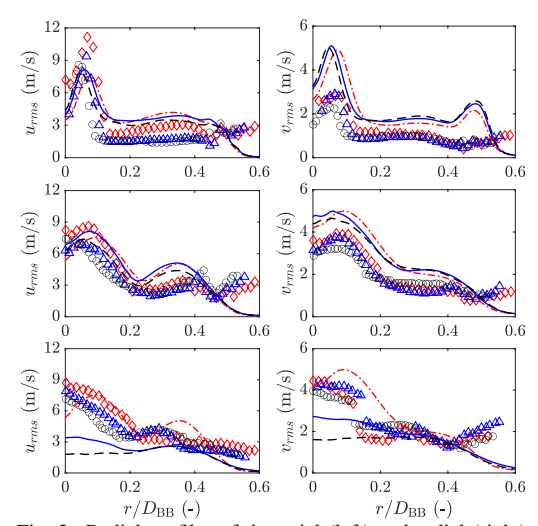


Fig. 2: Radial profiles of the axial (left) and radial (right) root-mean-square velocity fluctuations at three streamwise locations: $x/D_{\rm BB}=0.3$ (top), $x/D_{\rm BB}=0.9$ (middle), and $x/D_{\rm BB}=1.8$ (bottom). The lines and symbols are the same as in Fig. 1.

recirculation zone, and the third station is just downstream of the recirculation zone.

Overall, the LES results agree well with the experimental measurements. For the mean axial velocities, the most significant deviations occur at the most downstream station, and this is a result of the slight underprediction of the length of the recirculation zone, as discussed further below. In terms of the

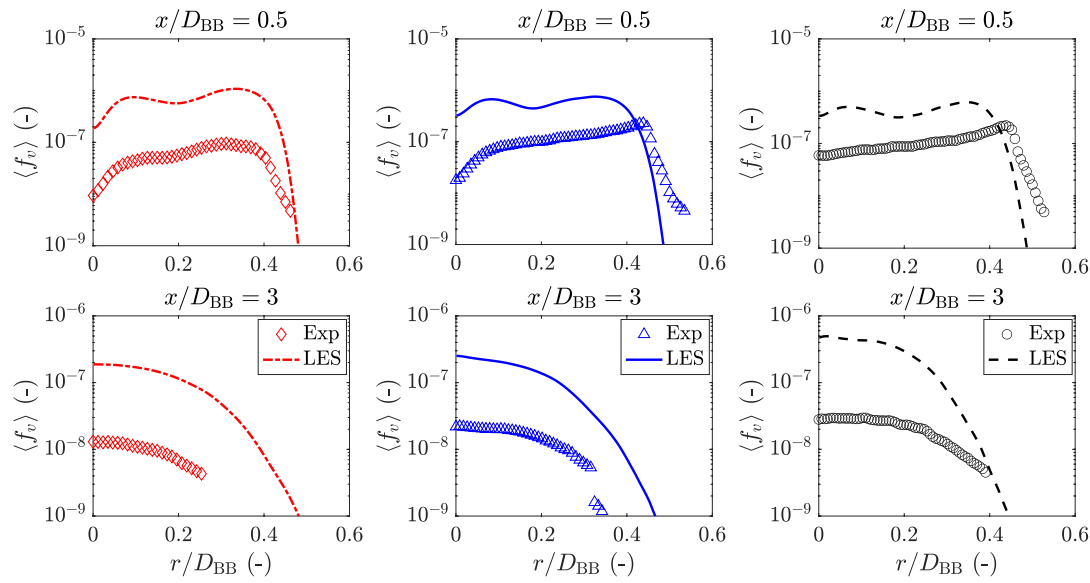


Fig. 3: Radial profiles of the mean soot volume fraction at two streamwise locations: $x/D_{\rm BB}=0.5$ (top) and $x/D_{\rm BB}=3$ (bottom). The columns correspond to the flames ENB-1 (left), ENB-2 (middle), and ENB-3 (right). The LES results are indicated with lines and the experimental measurements with symbols.

velocity fluctuations, the most upstream stations tend to be overpredicted, especially within the recirculation zone and in the outer shear layer between the recirculation zone and the coflow. The overprediction of the fluctuations in the outer shear layer at the most upstream station may be due to the excessive shear from the bulk inflow profile in the coflow: some boundary layer profile would reduce the shear so the production of turbulence in the outer shear layer.

In terms of the trends between the three flames, both the computations and the experiments predict more or less the same velocity profiles for the three flames. As discussed by Rowhani *et al.* [8], the most significant difference between the three cases then is the longer residence time in the larger recirculation zone in ENB-3, which has substantial effects on soot, as discussed next.

4.2. Soot volume fraction

Figure 3 shows the radial profiles of mean soot volume fraction in the three burners at two streamwise locations, one within the recirculation zone at $x/D_{\rm BB}=0.5$ and one just toward the beginning of the jet-like region at $x/D_{\rm BB}=3$. Figure 4 shows the corresponding root-mean-square (rms) soot volume fraction fluctuations at those locations. Overall, at both locations, the qualitative structure of the mean and rms soot volume fraction profiles is well captured, but the magnitude is overpredicted by a factor of a few (in the recirculation zone) up to an order of magnitude (at the beginning of the jet-like region). The overprediction of soot by a factor of a few is not inconsistent with previous results using the same modeling frame-

work in turbulent nonpremixed jet flames [6, 7, 16].

In the recirculation zone ($x/D_{\mathrm{BB}}\,=\,0.5$), in the experiments, the mean soot volume fraction increases radially outward and reaches its peak near $r/D_{\rm BB} \sim$ 0.5. The LES results tend to predict, on average, a more uniform radial profile of soot ($\langle f_v \rangle \simeq 0.5$ ppm) within the recirculation zone, but the structure is overall quite similar. The trend of rms fluctuations, however, is better reproduced, and the discrepancies of the LES results with the measurements decrease with radial distance. As the bluff body diameter $D_{\rm BB}$ increases (ENB-1 to ENB-3) so the residence time within the recirculation zone, the volume fraction increases, and this increase is reproduced by the LES model. On the other hand, for all three flames, the LES results exhibit a much sharper decrease in the mean soot volume fraction near the outer shear layer, although this is not the case with the rms fluctuations. In previous work, Mueller et al. [3] attributed a similar sharp decrease to the use of a bulk velocity profile for the coflow. However, such a trend seems inconsistent with the overpredicted velocity fluctuations, and additional investigations into the sensitivity of predictions to the coflow boundary condition is certainly warranted, as mentioned above.

In the jet-like region ($x/D_{\rm BB}=3$), both mean and rms soot volume fraction radially decrease, and the computational results capture this trend. In addition, as the bluff body diameter $D_{\rm BB}$ increases, both mean and rms soot volume fraction increase, and this quantitative trend is well captured by the LES model. At this location, soot is significantly reduced compared to the recirculation zone due to the high-strain environment of the neck region; this coupling between the

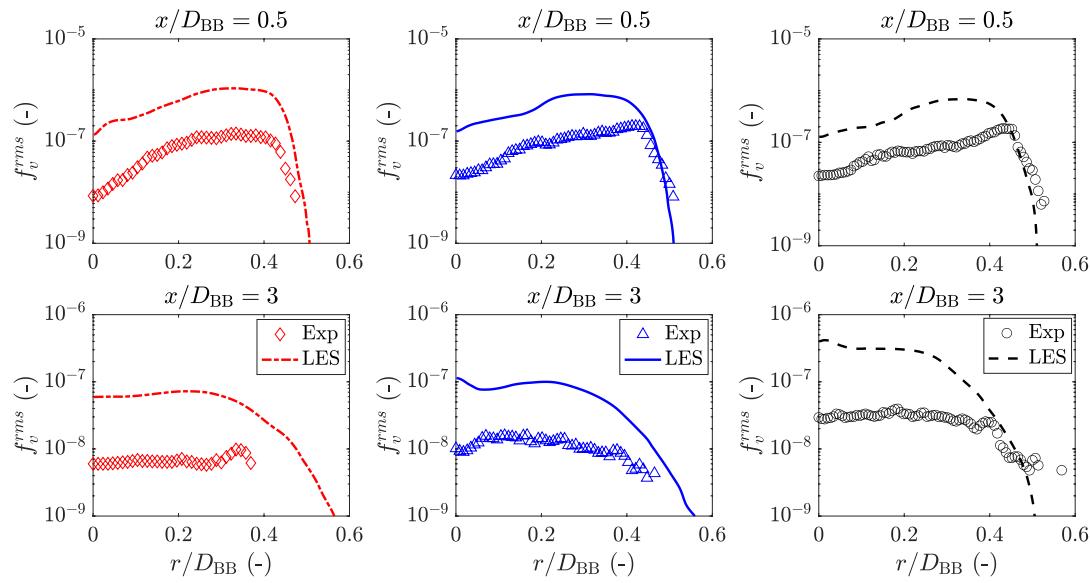


Fig. 4: Radial profiles of the root-mean-square soot volume fraction fluctuations at two streamwise locations: $x/D_{\rm BB}=0.5$ (top) and $x/D_{\rm BB}=3$ (bottom). The lines and symbols are the same as in Fig. 3.

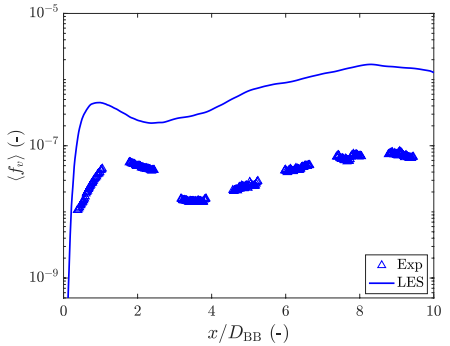


Fig. 5: Centerline profile of the mean soot volume fraction in flame ENB-2. The LES results are indicated with lines and the experimental measurements with symbols.

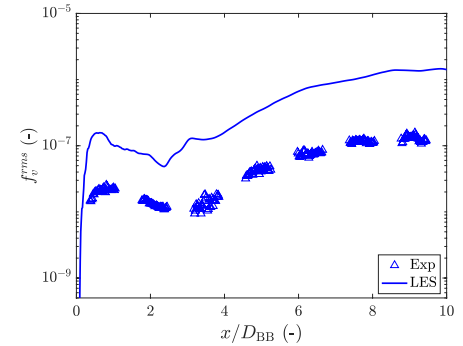


Fig. 6: Centerline profile of the root-mean-square soot volume fraction fluctuations in flame ENB-2. The lines and symbols are the same as in Fig. 5.

flow field and soot is discussed further below in the context of the source terms.

The centerline profiles of the mean and rms soot volume fraction are shown in Figs. 5 and 6 for ENB-2, respectively. The other two flames exhibit similar features and are not shown here for the sake of brevity. The soot volume fraction is large in the recirculation zone (up to $x/D_{\rm BB} \sim 1.5$), decreases in the high-strain neck region (1.5 $\lesssim x/D_{\rm BB} \lesssim 3.0$), and then increases again in the downstream jet-like region (beyond $x/D_{\rm BB} \sim 3.0$). These trends are captured by the LES model, although the computations, compared to the experiments, do tend to predict rather larger soot volume fractions in the downstream jet-like region relative to the recirculation zone. The rms fluctuations of the soot volume fraction exhibit

a similar, albeit smaller, overprediction. Clearly, the new soot subfilter PDF model for finite-rate oxidation of soot developed by Maldonado Colmán *et al.* [7] properly predicts significant soot in the downstream jet-like region, addressing the severe underprediction of soot with the model utilized in previous bluff body flames by Mueller *et al.* [3] and Deng *et al.* [4].

4.3. Soot source terms

With a model capable of predicting soot volume fraction in all regions of these bluff body flames, the results can be used to provide insights into the evolution of soot in the different regions of the flame and how this is influenced by the bluff body diameter.

To further characterize the turbulent nonpremixed bluff body flames, several soot-related quantities are

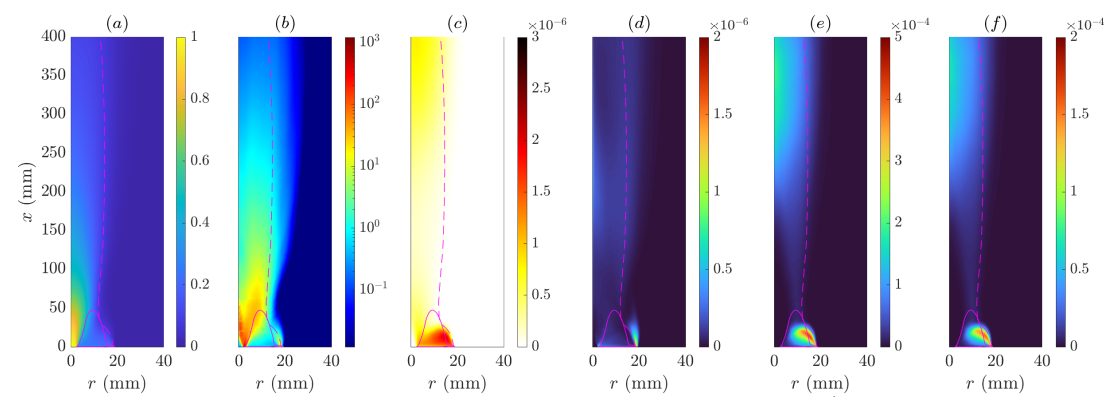


Fig. 7: Contours in ENB-1: (a) mixture fraction Z, (b) mixture fraction dissipation rate χ [s⁻¹]; (c) soot volume fraction f_v ; and soot source terms df_v/dt [s⁻¹] for (d) nucleation and condensation, (e) surface growth, and (f) oxidation (magnitude). The solid line corresponds to the iso-contour of zero axial velocity, and the dashed line corresponds to the iso-contour of stoichiometric mixture fraction.

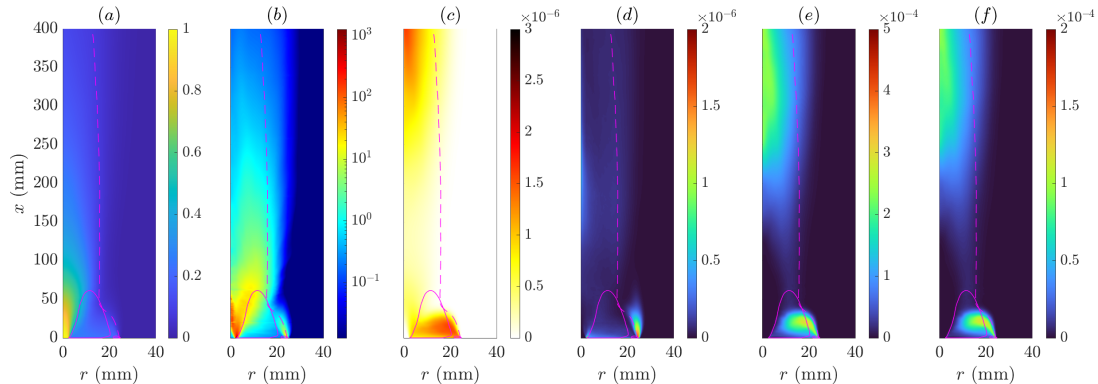


Fig. 8: Contours in ENB-2. The images correspond to the same quantities as in Fig. 7.

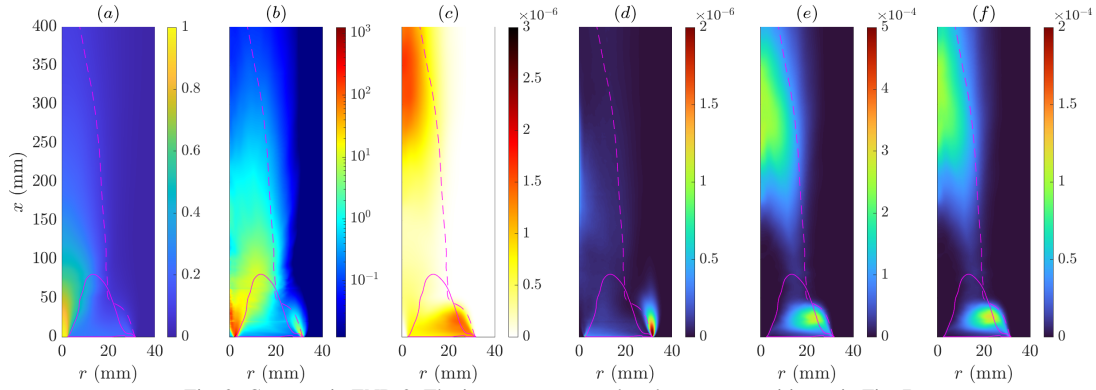


Fig. 9: Contours in ENB-3. The images correspond to the same quantities as in Fig. 7.

shown in Figs. 7–9 including the mixture fraction dissipation rate, the soot volume fraction, and the soot volume fraction source terms. In each figure, the continuous line delimits the contour where $\langle u \rangle = 0$ and defines the extent of the recirculation zone, while the dashed line is the stoichiometric mixture fraction contour ($Z_{\rm st}=0.078$).

The mean lengths of the recirculation zone obtained by LES in ENB-1, ENB-2, and ENB-3 correspond to the most downstream location of the $\langle u \rangle = 0$ contour and are 48 mm, 62 mm, and 82 mm, respectively. These recirculation zone lengths are approximately 25% shorter than the experimental measurements of Rowhani $et\ al.$ [8]. The sensitivity of the re-

circulation zone length to the inflow profile requires additional investigation.

The mixture fraction fields are shown in the (a)column of Figs. 7-9, where the fuel-rich mixtures that promote soot formation and growth spread further downstream and accumulate less in the recirculation zone as the diameter decreases. The mixture fraction dissipation rate fields are shown in the (b)column of Figs. 7-9. As observed also in the experiments [9], the regions of highest strain occur near the inner shear layer between the central jet and the recirculation zone. Despite the rich mixture fractions in this region, the high scalar dissipation rates suppress the formation of PAH, as indicated by the combined source term of nucleation and condensation (which is proportional to the square of the PAH mass fraction in the model) shown in the (d) column of Figs. 7-9. Conversely, near the outer shear layer, the dissipation rates are much smaller, and the combined rates of nucleation and condensation are larger, despite the leaner mixture fractions. Furthermore, with decreasing bluff body diameter, the dissipation rate increases and suppresses the formation of PAH so the combined rates of nucleation and condensation.

The mean soot volume fraction is shown in the (c)column of Figs. 7-9. Despite the very high mixture fraction dissipation rates, the soot volume fraction is actually relatively large near the inner shear layer and into the highly strained neck region just downstream of the recirculation zone. This indicates that soot is passively transported from the recirculation zone through the neck region (note that all source terms are zero in the neck region), a mechanism supported by the experimental measurements [9]. However, since there is a precipitous decrease in the soot volume fraction from the recirculation zone into the neck region (see Fig. 5), only a small portion of the soot formed in the recirculation zone escapes through the neck region; the remainder is oxidized near the outer shear layer, as indicated by the oxidation source term shown in the (f) column of Figs. 7-9. Since more soot forms in the larger recirculation zone of the ENB-3 flame with the larger bluff body, more soot also escapes the recirculation zone into the neck region.

Consistent with the previous bluff body flames [3, 4], both surface growth (the (e) column of Figs. 7-9) and oxidation peak near the outer shear layer. However, different from the previous bluff body flames [3, 4], the combined rates of nucleation and condensation peak not near the inner shear layer but rather the outer shear layer, as discussed above. This difference speaks to the sensitivity of bluff body flames to the inflow conditions including the fuel composition. Additionally, comparing the flame series, the surface growth (and oxidation) source term is actually faster with a smaller bluff body, but this is not sufficient to overcome the residence time advantage with the larger bluff body in terms of the production of soot.

Downstream of the neck region in the jet-like region, the soot volume fraction increases again

(Fig. 5). In the jet-like region, surface growth is the primary growth mechanism, and the combined rate of nucleation and condensation is negligible. This is contrary to previous computational results in turbulent nonpremixed jet flames [16] where the combined rates of nucleation and condensation are at least comparable to the surface growth rate. This means that the soot growth mechanism is very different in the jet-like region of the bluff body flames compared to jet flames. Expanding upon the soot dynamics in the recirculation zone and the neck region, the soot that escapes through the neck region then grows again by surface growth in jet-like region; very little soot is formed in the jet-like region. In other words, the increase in the soot volume fraction in the jet-like region occurs only because soot is present that escaped from the recirculation zone to then grow again by surface growth. The source terms are largest in the flames with the largest bluff body diameter (note that the maximum occurs beyond an axial distance of 400mm in ENB-3) since more soot escapes the recirculation zone and the source terms of surface growth and oxidation proportional to the amount of soot.

With the previously considered soot subfilter PDF model that overpredicts oxidation [5], no soot was able to escape the recirculation zone into the neck region and ultimately the jet-like region where it grows again. The advances in the soot subfilter PDF to correct the overprediction of oxidation [6, 7] actually enable the prediction of soot escaping the recirculation zone to evolve downstream, consistent with the experimental measurements.

5. Conclusions

LES was used to investigate soot evolution in a series of three new turbulent nonpremixed bluff body flames with different bluff body diameters. The LES relies on a new soot subfilter PDF model that accounts for the influence of finite-rate oxidation of soot on its distribution with respect to mixture fraction and corrects a significant overprediction of oxidation with previous soot subfilter PDF models that have been used to investigate soot evolution in turbulent non-premixed bluff body flames.

Compared to the experimental measurements, the LES results showed generally good agreement with experimental measurements of both the flow field and the soot volume fraction, although the latter was moderately overpredicted across the flame series. Consistent with the experimental measurements, for the flame with the largest bluff body diameter, the large recirculation zone with long residence times promoted the most soot formation in the recirculation zone. A small fraction of this soot escapes the recirculation zone unoxidized where it is passively transported through the high-strain neck region and into the downstream jet-like region. In the jet-like region, virtually no new soot is formed; instead, the soot that escapes from the recirculation zone grows via acetylene-based surface growth, a very different mechanism than most turbulent nonpremixed jet flames.

Prediction of this soot evolution mechanism relies on the accurate prediction of the oxidation of soot in the recirculation zone and could not be predicted without the new soot subfilter PDF model that has been utilized in this work. This conclusion reinforces the notion that soot evolution in turbulent reacting flows requires very accurate models for small-scale soot-turbulence-chemistry interactions for not only accurate predictions but also even discovering basic mechanisms.

Acknowledgments

The authors gratefully acknowledge funding from the National Science Foundation, Award CBET-2028318. The simulations presented in this article were performed on computational resources supported by the Princeton Institute for Computational Science and Engineering (PICSciE) and the Princeton University Office of Information Technology's Research Computing department.

References

- H. Koo, M. Hassanaly, V. Raman, M. E. Mueller, K. P. Geigle, Large-Eddy Simulation of soot formation in a model gas turbine combustor, J. Eng. Gas Turb. Power 139 (2017) 031503.
- [2] C. Eberle, P. Gerlinger, K. P. Geigle, M. Aigner, Toward finite-rate chemistry large-eddy simulations of sooting swirl flames, Combust. Sci. Tech. 190 (2018) 1194–1217.
- [3] M. E. Mueller, Q. N. Chan, N. H. Qamar, B. B. Dally, H. Pitsch, Z. T. Alwahabi, G. J. Nathan, Experimental and computational study of soot evolution in a turbulent nonpremixed bluff body ethylene flame, Combust. Flame 160 (2013) 1298–1309.
- [4] S. Deng, M. E. Mueller, Q. N. Chan, N. H. Qamar, B. B. Dally, Z. T. Alwahabi, G. J. Nathan, Hydrodynamic and chemical effects of hydrogen addition on soot evolution in turbulent nonpremixed bluff body ethylene flames, Proc. Combust. Inst. 36 (2017) 807– 814
- [5] M. E. Mueller, H. Pitsch, Large Eddy Simulation subfilter modeling of soot-turbulence interactions, Phys. Fluids 23 (2011) 115104.
- [6] S. Yang, J. K. Lew, M. E. Mueller, Large Eddy Simulation of soot evolution in turbulent reacting flows: Presumed subfilter PDF model for soot-turbulencechemistry interactions, Combust. Flame 209 (2019) 200–213.
- [7] H. Maldonado Colmán, A. Attili, M. E. Mueller, Large Eddy Simulation of nonpremixed turbulent sooting flames: Presumed subfilter PDF model for finite-rate oxidation of soot, Combust. Flame (2022) Under review.
- [8] A. Rowhani, Z. W. Sun, P. R. Medwell, Z. T. Alwahabi, G. J. Nathan, B. B. Dally, Effects of the bluff-body diameter on the flow-field characteristics of non-premixed turbulent highly-sooting flames, Combust. Sci. Technol. (2019) 1–19.
- [9] A. Rowhani, Z. Sun, P. R. Medwell, G. J. Nathan,B. B. Dally, Soot-flowfield interactions in turbulent

- non-premixed bluff-body flames of ethylene/nitrogen, Proc. Combust. Inst. 38 (2021) 1125–1132.
- [10] M. E. Mueller, G. Blanquart, H. Pitsch, A joint volume-surface model of soot aggregation with the method of moments, Proc. Combust. Inst. 32 (2009) 785–792.
- [11] M. E. Mueller, G. Blanquart, H. Pitsch, Hybrid Method of Moments for modeling soot formation and growth, Combust. Flame 156 (2009) 1143–1155.
- [12] M. E. Mueller, G. Blanquart, H. Pitsch, Modeling the oxidation-induced fragmentation of soot aggregates in laminar flames, Proc. Combust. Inst. 33 (2011) 667– 674.
- [13] M. E. Mueller, H. Pitsch, LES model for sooting turbulent nonpremixed flames, Combust. Flame 159 (2012) 2166–2180.
- [14] R. S. Barlow, A. N. Karpetis, J. H. Frank, J.-Y. Chen, Scalar profiles and no formation in laminar opposedflow partially premixed methane/air flames, Combust. Flame 127 (2001) 2102–2118.
- [15] G. L. Hubbard, C. L. Tien, Infrared mean absorption coefficients of luminous flames and smoke, J. Heat. Transf. 100 (1978) 287–305.
- [16] S. Yang, J. K. Lew, M. E. Mueller, Large Eddy Simulation of soot evolution in turbulent reacting flows: Strain-Sensitive Transport Approach for Polycyclic Aromatic Hydrocarbons, Combust. Flame 220 (2020) 219–234.
- [17] M. Ihme, H. Pitsch, Modeling of radiation and nitric oxide formation in turbulent nonpremixed flames using a flamelet/progress variable formulation, Phys. Fluids 20 (5) (2008) 055110.
- [18] A. W. Cook, J. J. Riley, A subgrid model for equilibrium chemistry in turbulent flows, Phys. Fluids 6 (1994) 2868–2870.
- [19] S. B. Pope, The evolution of surfaces in turbulence, Int. J. Eng. Sci. 26 (1988) 445–469.
- [20] O. Desjardins, G. Blanquart, G. Balarac, H. Pitsch, High order conservative finite difference scheme for variable density low mach number turbulent flows, J. Comput. Phys. 227 (2008) 7125–7159.
- [21] J. F. MacArt, M. E. Mueller, Semi-implicit iterative methods for low mach number turbulent reacting flows: Operator splitting versus approximate factorization, J. Comput. Phys. 326 (2016) 569–595.
- [22] M. Germano, U. Piomelli, P. Moin, W. H. Cabot, A dynamic subgrid-scale eddy viscosity model, Phys. Fluids 3 (1991) 1760–1765.
- [23] C. Meneveau, T. S. Lund, W. H. Cabot, A Lagrangian dynamic subgrid-scale model of turbulence, J. Fluid Mech. 319 (1996) 353–385.
- [24] H. Pitsch, FlameMaster: A C++ computer program for 0D combustion and 1D laminar flame calculations, URL: http://www.itv.rwthaachen.de/en/downloads/flamemaster 81 (1998).
- [25] G. Blanquart, P. Pepiot-Desjardins, H. Pitsch, Chemical mechanism for high temperature combustion of engine relevant fuels with emphasis on soot precursors, Combust. Flame 156 (2009) 588–607.
- [26] K. Narayanaswamy, G. Blanquart, H. Pitsch, A consistent chemical mechanism for oxidation of substituted aromatic species, Combust. Flame 157 (2010) 1879–1898.